Chemical Science

EDGE ARTICLE

View Article Online
View Journal | View Issue

Cite this: *Chem. Sci.*, 2019, **10**, 4876

All publication charges for this article have been paid for by the Royal Society of Chemistry

Monitoring the dynamics of hemeoxygenase-1 activation in head and neck cancer cells in real-time using plasmonically enhanced Raman spectroscopy†

Sajanlal R. Panikkanvalappil,[a] Chakravarthy Garlapati,[b] Nasrin Hooshmand,[a] Ritu Aneja[b] and Mostafa A. El-Sayed *[a]

We report for the first time the usage of plasmonically enhanced Raman spectroscopy (PERS) to directly monitor the dynamics of pharmacologically generated hemeoxygenase-1 (HO-1) by evaluating the kinetics of formation of carbon monoxide (CO), one of the metabolites of HO-1 activation, in live cells during cisplatin treatment. Being an endogenous signaling molecule, CO plays an important role in cancer regression. Many aspects of HO-1's and CO's functions in biology are still unclear largely due to the lack of technological tools for the real-time monitoring of their dynamics in live cells and tissues. In this study, we found that, together with nuclear region-targeted gold nanocubes (AuNCs), cisplatin treatment can dramatically trigger the activation of HO-1 and thereby the rate and production of CO in mammalian cells in a dose-dependent manner. Though quantitative molecular data revealed that a lower concentration of cisplatin up-regulates HO-1 expression in cancer cells, PERS data suggest that it poorly facilitates the activation of HO-1 and thereby the production of CO. However, at a higher dose, cisplatin along with AuNCs could significantly enhance the activation of HO-1 in cancer cells, which could be probed in real-time by monitoring the CO generation by using PERS. Under the same conditions, the rate of formation of CO in healthy cells was relatively higher in comparison to the cancer cells. Additionally, molecular data revealed that AuNCs have the potential to suppress the up-regulation of HO-1 in cancer cells during cisplatin treatment at a lower concentration. As up-regulation of HO-1 has a significant role in cell adaptation to oxidative stress in cancer cells, the ability of AuNCs in suppressing the HO-1 overexpression will have a remarkable impact in the development of nanoformulations for combination cancer therapy. This exploratory study demonstrates the unique possibilities of PERS in the real-time monitoring of endogenously generated CO and thereby the dynamics of HO-1 in live cells, which could expedite our understanding of the signaling action of CO and HO-1 in cancer progression.

Received 7th January 2019
Accepted 21st March 2019

DOI: 10.1039/c9sc00093c

rsc.li/chemical-science

Introduction

Head and neck cancer (HNC) is one of the most commonly occurring malignancies worldwide, which encompasses a site-specific heterogeneous group of cancers arising from the upper aerodigestive tract.[1,2] Most of the HNCs begin in the squamous cells, hence they represents more than 90% of cancer incidents.[3] Despite recent advances in cancer theranostics, the optimal treatment for locally advanced HNC is limited to chemo-radio therapeutic approaches.[4,5] Platinum-based chemotherapy is considered as the traditional first-line treatment for metastatic squamous-cell head and neck carcinoma.[6] *cis*-Diamminedichloroplatinum II (Cisplatin) is an effective and established chemotherapeutic drug being used for HNCs.[7,8] Even though, the formation of cisplatin/DNA adducts as well as the accumulations of reactive oxygen species (ROS) are widely accepted as the key cytotoxic mechanisms of cisplatin toxicity, their exact role in inducing toxicity to the healthy and cancer cells are still poorly understood.[9] Furthermore, the underlying mechanisms of cisplatin toxicity due to a myriad of caspase-triggered apoptotic pathways still remain unclear. As a result, severe side effects and acquired drug resistance have been associated with cisplatin chemotherapy.[10,11]

Many of the recent studies suggest that hemeoxygenase-1 (HO-1), a cytoprotective enzyme, which degrades heme into bioactive carbon monoxide (CO), biliverdin and ferrous ion, is overexpressed in many cancer cells including HNCs and plays a significant role in maintaining tumour cell survival and

[a]*Laser Dynamics Laboratory, School of Chemistry and Biochemistry, Georgia Institute of Technology, Atlanta, Georgia 30332, USA. E-mail: melsayed@gatech.edu*

[b]*Georgia State University, Department of Biology, Atlanta, GA, USA*

† Electronic supplementary information (ESI) available: TEM image of AuNCs, extinction spectra of AuNCs, additional PERS data, and dark field images, *in silico* analysis of HO-1 expression. See DOI: 10.1039/c9sc00093c

progression through promoting angiogenesis and distant metastases as well as chemotherapeutic resistance.[12–15] As most of the functions of HO-1 are known to be mediated by its metabolites, especially CO, unravelling the role of chemotherapeutically generated CO would provide a better understanding of the molecular mechanisms behind the cisplatin-induced HO-1 activity modulation on cellular responses in HNCs. Even though many studies suggest the role of CO as a mediator of angiogenesis,[13] a precise mechanism of action of this process is yet to be discovered.[16] Many aspects of CO signalling in live cells are still unclear largely due to the lack of technological tools for the real-time monitoring of CO dynamics in mammalian cells. Plasmonically-enhanced Raman spectroscopy (PERS), which takes advantage of the enhanced electromagnetic fields[17,18] in the nanogap between assembled plasmonic gold nanoparticles, has been widely explored to obtain the vibrational fingerprint of the biological environment around the nanoparticles, within living cells.[19–22]

Herein, we report for the first time the usage of plasmonically enhanced Raman scattering properties of gold nanocubes to directly monitor the dynamics of HO-1 activation in live cells during cisplatin treatment. Activation of HO-1 during cisplatin treatment was evaluated by monitoring CO evolution, one of the metabolites of HO-1 activation, using PERS. Furthermore, the expression of HO-1 under various conditions was quantitatively analysed by conducting western blotting. During this study, we found that the concentration of cisplatin together with gold nanoparticles can dramatically affect the expression of HO-1 as well as the rate of its activation and subsequent production of CO in mammalian cells. Real-time monitoring of generation of CO in live cells will be a promising strategy for understanding the effects of CO and thereby HO-1 on cellular signalling.

Results and discussion

During our studies on the mechanism of action of cisplatin-induced cell death, we made a novel observation using PERS that the expression and activation of HO-1 can be significantly altered by the cell internalized gold nanoparticles as well as the concentration of the anticancer drug. For this study, we used PEG/RGD/NLS/gold NCs (AuNCs) with an average diameter of 40 $\pm$ 7 nm as the PERS nanoprobe due to the high electromagnetic field around the surface and subsequent enhanced PERS activity of AuNCs.[20,23] The extinction spectra and corresponding TEM images of these AuNCs are given in the Fig. S1 in the ESI.† While PEGylation of nanoparticles improve their stability and cell viability, it also reduces the nonspecific protein binding to their surface.[24–26] Whereas, RGD and NLS facilitated the cellular uptake of NCs through receptor-mediated endocytosis and their localization at the nuclear region, respectively.[19,25,27,28] To evaluate the role of cisplatin on the expression of HO-1 in human oral squamous cell carcinoma (HSC-3) cancer cells, which were pre-incubated with AuNCs, we treated these cells with cisplatin at different concentrations. Exposure of 75 μM of cisplatin to the AuNCs-treated HSC-3 cells triggered gradual apoptosis of the cells, which was evident from the dark-field images and PERS spectra (Fig. S2 in the ESI†). After 12 h of drug treatment, characteristic Raman bands corresponding to phenylalanine ring vibrations, usually appear at around 1001 cm^{-1} and 1584 cm^{-1}, became prominent in the PERS spectra (see Fig. S2 in the ESI†). Our earlier studies showed that these bands become prominent during cell death.[29,30] In addition to these cell death associated Raman bands, dark-field images showed the blebbing of the cellular membrane after 15 h, which also indicates the apoptotic cell death.[30]

While real-time PERS spectra showed a similar trend as shown in our previous studies at a concentration of 75 μM,[31] at a higher dose of cisplatin (200 μM), an entirely new spectral trend in the PERS spectra was observed (Fig. 1). Interestingly, at a cisplatin concentration of 200 μM, a new Raman band emerged at ~2115 cm^{-1}. This region has been considered as the Raman-silent window of biomolecules, where natural cellular molecules do not produce prominent Raman signals in this silent region.[32,33] From our detailed studies (described later in the text) we found that the observed Raman band corresponds to the stretching vibration of carbon monoxide (ν_{CO}),[34–36] a by-product of the heme metabolism, generated within the cells by the upregulation and activation of HO-1 during the drug treatment. We also noted that this band appears at the early stages of drug treatment as multiple bands between 2075 and 2180 cm^{-1}, which are attributed to the possible conformation-dependent linear and bridged interactions between the AuNC metal surface with CO (Fig. 1D).[37,38] Tentative assignments of the main Raman bands relevant to this study are given in Table 1. Furthermore, we illustrated the concentration-dependence of cisplatin on the activation of HO-1 and subsequent emergence of ν_{CO} vibration by conducting similar experiments at various cisplatin concentrations (125 μM and 300 μM). Time dependent PERS spectra as well as a plot showing the normalized intensities of vibrations of ν_{CO} collected as a function of cisplatin treatment time at different drug concentrations are given in Fig. S3 in the ESI.† From this study, we found that the rate of HO-1 activation and formation of CO is highly dependent on the concentration of the drug, and it is prominent at higher concentrations.

Since CO has a strong affinity towards the metal surface, it can form the M–CO bond in the lower wavenumber region of the PERS spectrum.[37,39] Interestingly, together with the emergence of the ν_{CO} Raman band at a higher wavenumber region, the gradual appearance of M–CO stretching vibration (ν_{M-CO}) at ~484 cm^{-1} was also apparent. This observation points towards the fact that enzymatically generated CO within the HSC-3 cell during cisplatin treatment indeed interacts with the AuNCs surface. A gradual reduction in the intensity of the disulfide band (~504 cm^{-1}) with simultaneous formation of the ν_{M-CO} band at ~484 cm^{-1} further validates the presence of CO at the close proximity of the plasmonic nanoparticle. Nevertheless, C–S vibration (~655 cm^{-1}) was retained in the spectra even after the interaction of CO with the nanoparticle surface. Even though there are several other Raman bands that showed significant modifications during the cisplatin treatment, we focused more on the aforementioned vibrations, as the modifications to them were more consistent and reliable.

Following the encouraging results obtained from our real-time PERS studies as mentioned above, we further validated

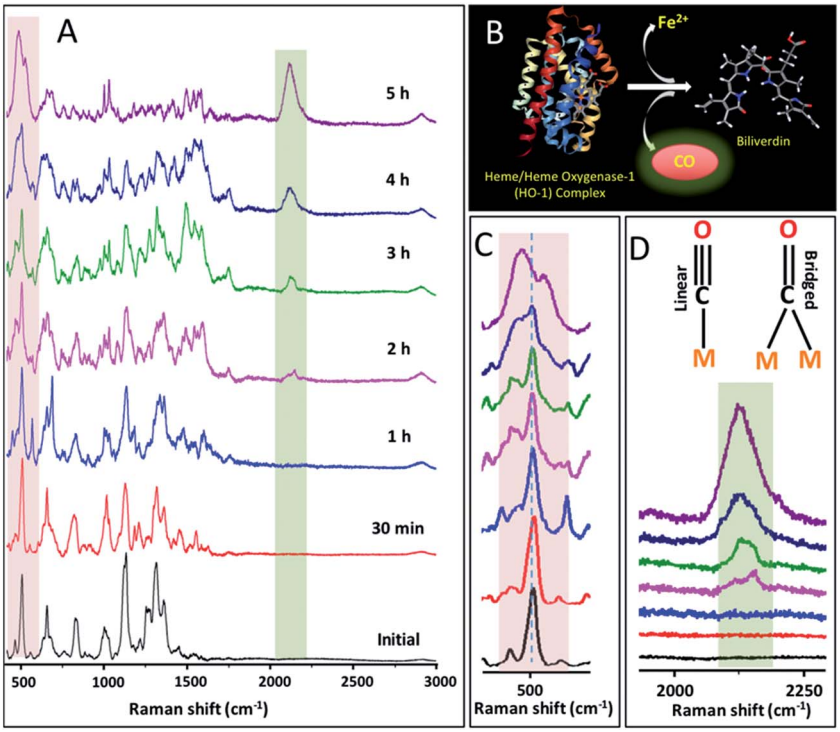

Fig. 1 (A) Real-time PERS spectra taken from PEG/RGD/NLS/AuNCs-internalized HSC-3 cells while being treated with cisplatin (200 μM). (B) Schematic representation showing the enzymatic conversion of heme by HO-1. (C and D) are the enlarged views of the PERS spectra showing the disulfide vibration (~504 cm^{-1}) in proteins and ν_{CO} (~2115 cm^{-1}) in CO. Two possible metal carbonyl interactions are also shown in panel (D).

the extent of CO contribution to the PERS band observed at 2115 cm^{-1} by conducting control experiments. Here, we treated the HSC-3 cells (having internalized AuNCs) with CO-releasing molecules, CORM-3 ($Ru(CO)_3Cl(glycinate)$). CORM-3 is a water-soluble molecule, which can liberate CO molecules to the biological systems in a controlled manner.[40,41] PERS spectra of CORM-3, as well as HSC-3 cells (with internalized AuNCs) treated with CORM-3 and cisplatin, are given in Fig. 2. The Raman spectral features corresponding to endogenously generated CO obtained from the cisplatin-treated HSC-3 cells showed noteworthy resemblance to the spectrum of CORM-3 internalized HSC-3 cells, which further validates that the observed vibration found at ~2115 cm^{-1} is mainly due to endogenously-generated CO by the HO-1 activation during the cisplatin treatment.

Taking into consideration that a higher dose of cisplatin (200 μM) can enhance the activation of HO-1 and the production of CO in HSC-3 cancer cells, we further investigated the HO-1 over expression capability of docetaxel, an antimitotic chemotherapeutic drug that inhibits the microtubule dynamics.[42] Although, administration of 200 μM of docetaxel-triggered apoptosis in HSC-3 cells within one hour (Fig. S4 in the ESI†) of administration, characteristic Raman vibrations corresponding to CO generated by the upregulation of HO-1 was not evident in the PERS spectra. This suggests that the HO-1 overexpression and its activation largely depend on the mechanism of action of the drug molecules. Additionally, the intensity of the ν_{CO} vibration during the control PERS spectra collected from HSC-3 cells in the absence of cisplatin treatment (Fig. S5 in the ESI†) was negligible, which further validates that

Table 1 Tentative assignment of relevant Raman bands in the PERS spectra

Wavenumber (cm^{-1})	Component	Tentative assignments of PERS bands
475–490	CO	Metal–CO stretching (ν_{M-CO})
495–510	Protein	–S–S–
620–660	Protein	–C–S–
1000–1005	Protein	Ring breathing vibration of phenylalanine
1012–1030	Protein	In-plane bending mode of phenylalanine and ring breathing vibration of tryptophan
1100–1140	Lipid and protein	–C–N– vibration of proteins and conformation-dependent vibrations of lipids
1210–1300	Protein	Amide III (α-helix, β-pleated sheet, and random coil)
1300–1325	Protein and lipid	$-CH_2$ twist
1584	Protein	Phenylalanine
1850–2180	CO	C–O stretching (ν_{CO}); linear and bridged

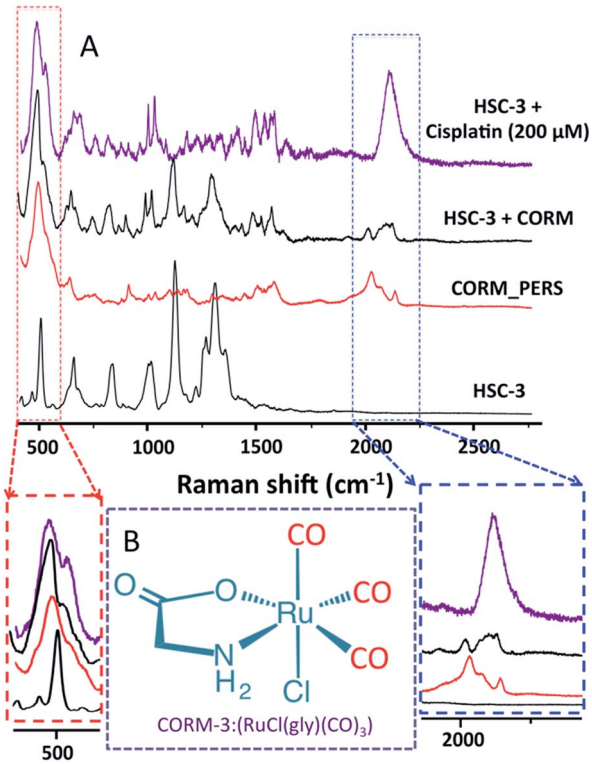

Fig. 2 (A) Comparison of PERS spectra of CORM-3 with the spectra collected from CORM-3 as well as cisplatin-incubated HSC-3 cells (pre-incubated with AuNCs). Spectral regions corresponding to ν_{M-CO} vibration (left) and ν_{CO} (right) are enlarged for clarity. Panel (B) shows the molecular structure of CORM-3.

the activation of HO-1 is indeed necessary to be able to monitor the Raman vibration of endogenously generated CO. It is likely that the size, shape, composition, and surface ligand characteristics of the nanomaterials can possibly modulate HO-1 activation as these factors largely affect the endocytosis of nanoparticles. In addition, PEG/RGD/NLS/gold nanospheres (AuNSs) under the same conditions as that of AuNCs during cisplatin treatment also resulted in the activation of HO-1 and subsequent formation of the CO Raman bands. However, the intensity of the ν_{CO} vibration was relatively lower compared to AuNCs (Fig. S6 in the ESI†).

In order to further access, the metabolic activity of healthy cells towards cisplatin in comparison to cancer cells, PERS experiments were conducted on healthy human keratinocyte (HaCaT) cells by following the same experimental conditions used in the case of HSC-3 cells (Fig. 3A–C). Even though a similar trend was observed in the activation of OH-1 and emergence of the ν_{CO} Raman band at 2115 cm^{-1} at a higher cisplatin concentration, a significant increase in the rate of appearance of the CO Raman bands was evident (Fig. 3D) in HaCaT cells. These results showed that the rate of expression and activation of HO-1 in HaCaT cells was higher than those in HSC-3 cells. We also noticed that nearly 1.5-fold higher cell death was evident in HSC-3 compared to the HaCaT cell line after 24 h of cisplatin treatment (Fig. 3E and F). This result is consistent with the observations of Wegiel B *et al.*[15]

In order to quantitatively investigate the cisplatin-induced HO-1 over expression as well as the susceptibility of AuNCs to facilitate the expression of HO-1, western blot is performed

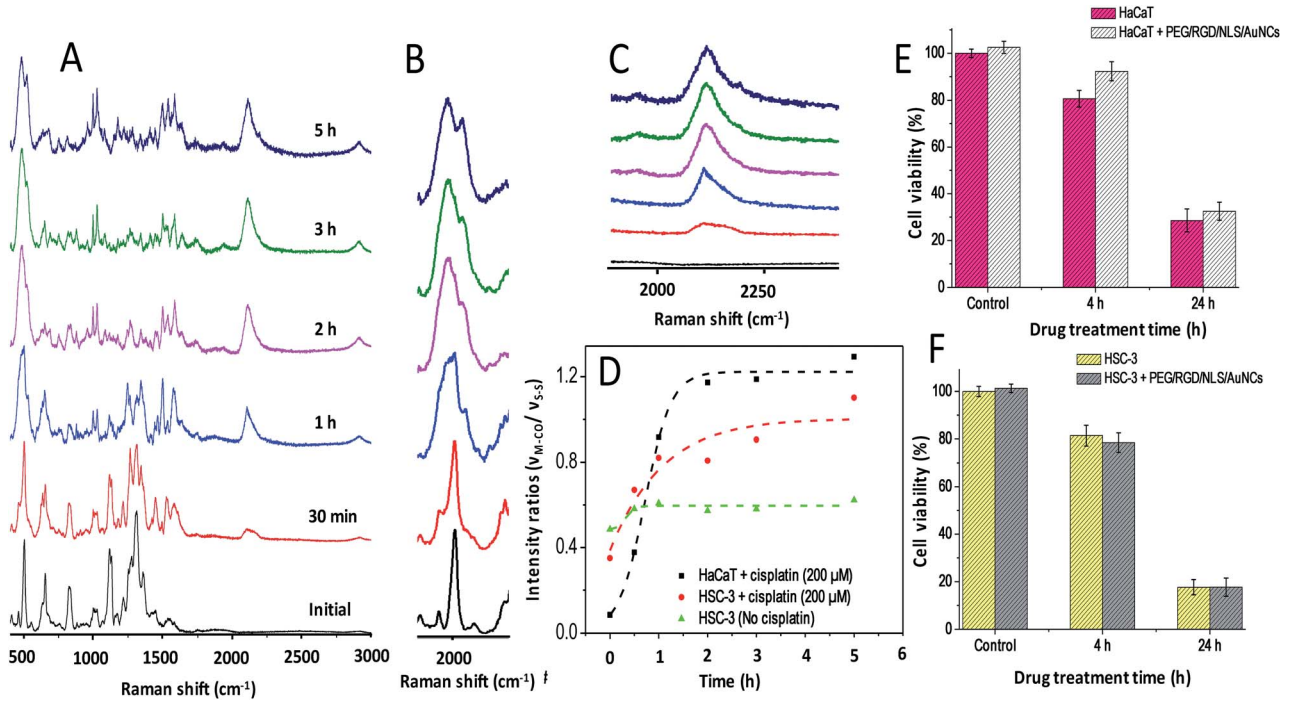

Fig. 3 (A) Real-time PERS spectra taken from PEG/RGD/NLS/AuNCs-internalized HaCaT cells while being treated with cisplatin (200 μM). (B and C) are the enlarged view of the PERS spectra showing the disulfide vibration (~504 cm^{-1}) in proteins and carbonyl vibration (~2115 cm^{-1}) in CO. (D) Plot showing the ratio between the ν_{M-CO} vibration and S–S vibration in HSC-3 and HaCaT cells during cisplatin treatment (200 μM). (E and F) show the cell viability for HaCaT and HSC cells treated with 200 μM cisplatin for 4 h and 24 h.

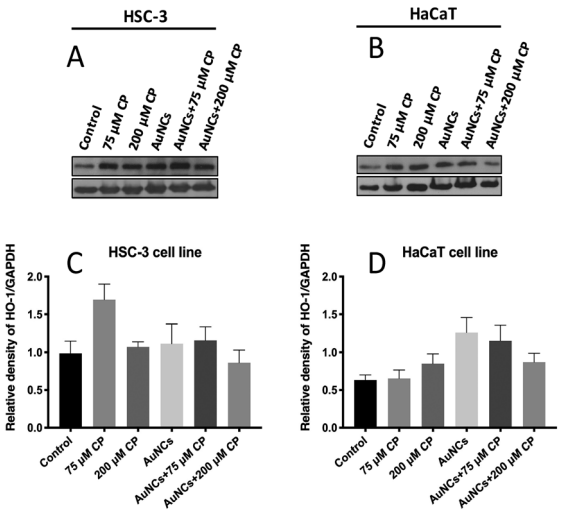

Fig. 4 Western blot analysis of HO-1 protein levels in HSC-3 (A and C) and HaCaT cells (B and D) under different experimental conditions. Cells were treated with 75 μM and 200 μM of cisplatin for 4 h in the presence and absence of AuNCs. Cells not exposed to AuNCs and cisplatin served as a negative control. The treated and untreated cells were lysed and cell extract subjected to western blots with anti-HO-1 antibodies. The α-GAPDH used as a loading control.

(Fig. 4) at cisplatin concentrations of 75 μM and 200 μM in the presence and absence of AuNCs on HSC-3 and HaCaT cells. From the western blot analysis, it is clear that AuNCs act as the suppressor of HO-1 expression in HSC-3 cells during the treatment of cisplatin at a concentration of 75 μM. However, at a higher concentration of cisplatin (200 μM), HO-1 upregulation was not as significant as at 75 μM and was almost identical to the control cells. Interestingly, our Raman study confirmed that even though lower cisplatin treatment (75 μM) upregulates the HO-1 expression, it substantially suppresses the activation of HO-1 and subsequent production of CO, one of the by-products of HO-1 activation. At the same time, treatment with a higher cisplatin concentration (200 μM) significantly enhanced the activation of HO-1 and produced CO in large quantities (evident from PERS spectra). This result points towards the fact that AuNCs can possibly downregulate the expression of HO-1 (a cytoprotective enzyme) in HSC-3 cancer cells, which has huge potential in reducing the proliferation of cancer cells in chemotherapeutic interventions.

Conclusions

We have demonstrated that PERS can be used to monitor the dynamics of HO-1 in mammalian cells by monitoring endogenously generated CO, one of its metabolites that provide a direct measure of HO-1 activation. Formation of CO during cisplatin treatment in cancerous HSC-3 cells and healthy HaCaT cells was confirmed by monitoring the characteristic ν_{CO} vibration found at the Raman silent region of biomolecules (~2115 cm^{-1}). Compared to a lower dose (75 μM), treatment with a higher dose (200 μM) of cisplatin along with AuNCs significantly enhanced the activation of HO-1. From PERS studies, we noticed that rate of activation of HO-1 and subsequent production of CO was higher in HaCaT cells compared to in HSC-3 cells. Western blotting studies revealed that though the lower concentration of cisplatin upregulates the HO-1 expression in HSC-3 cancer cells AuNCs has the potential to suppress the overexpression of HO-1 in HSC-3 cancer cells.

Experimental

(a) Materials

Hydrogen tetrachloroaurate trihydrate aqueous solution ($HAuCl_4 \cdot 3H_2O$), sodium borohydride ($NaBH_4$), $AgNO_3$, ascorbic acid, cetyltrimethylammonium bromide (CTAB), and trisodium citrate were purchased from Sigma-Aldrich USA. Cisplatin was purchased from Alfa Aesar (Lancashire, U.K.). Custom-made peptides such as RGD (RGDRGDRGDRGDPGC) and NLS (CGGGPKKKRKVGG) were purchased from GenScript USA, Inc. Thiol-modified methoxypolyethylene glycol (mPEG-SH, MW 5000) was obtained from Laysan Bio, Inc.

(b) Instrumentation

The transmission electron microscopy (TEM) image was taken using a JEOL 100CX-2 microscope. The average diameter of the AuNCs was determined using ImageJ software. Dark-field images and PERS spectra from the human oral squamous cell carcinoma (HSC) and human keratinocyte (HaCaT) cells were collected using a Renishaw inVia Raman microscope coupled with a Leica microscope. A 785 nm diode laser (~5.9 mW) was used for the PERS measurements.

(c) Synthesis of gold nanocubes (NCs) and gold nanospheres (NSs)

Gold nanocubes were prepared by following the modified seed-mediated method reported by Murphy *et al.*[43] The seed nanoparticles were prepared by the reduction of 250 μL of $HAuCl_4 \cdot 3H_2O$ (10 mM) in 7 mL of 100 mM CTAB solution in deionized water (DI) by 600 μL of an ice cold 10 mM $NaBH_4$ solution under stirring for 2 minutes. After one hour 0.35 mL of tenfold diluted seed solution was allowed to grow for 4 h in a growth solution. The growth solution was prepared by mixing CTAB solution (2.916 g dissolved in 400 mL DI water) with $HAuCl_4 \cdot 3H_2O$ solution (0.0394 g dissolved in 143 mL DI water) followed by adding 6 mL (1 M) ascorbic acid. The resultant CTAB stabilized gold nanocubes were purified by centrifugation (8000 rpm for 10 min) and redispersion in DI water. Gold nanospheres (NSs) were synthesized by adding 0.2% of trisodium citrate trihydrate (2.5 mL) into the boiling solution of 140 mL of 1% $HAuCl_4 \cdot 3H_2O$ in DI water. The solution was heated until it turned to red wine color.

(d) Preparation of PEG/RGD/NLS-functionalized gold nanocubes (AuNCs) and gold nanospheres (AuNSs)

Gold NCs were functionalized with mPEG-SH by incubating 15 mL of 0.2 nM NCs solution with 90 μL of mPEG-SH (1 mM) for 24 h. Similarly, AuNSs were conjugated with mPEG-SH by incubating 5 mL of 3 nM AuNSs solution with 30 μL of 1 mM mPEG-SH solution for 24 h. Afterwards, the PEGylated

nanoparticles were treated with RGD and NLS with a ratio of 4 : 10 to yield PEG/RGD/NLS-functionalized nanoparticles. The nanoparticles at different stages of preparation were purified by centrifugation to remove unbound ligands.

(e) Cell lines, media and antibodies

HSC and HaCaT cells were cultured in Dulbecco's modified Eagles' medium (DMEM, Mediatech), with phenol red, supplemented with 10% v/v fetal bovine serum (FBS, Mediatech) and 1% antimycotic solution (Mediatech) in a 37 °C, 5% CO_2 humidified incubator. For the PERS studies, the mammalian cells were grown on glass coverslips in complete growth medium in an incubator at 37 °C for 24 h. Afterwards, the cells were incubated with 0.075 nM of PEG/RGD/NLS-functionalized nanoparticles (AuNCs), diluted in supplemented DMEM cell culture medium, for 24 h. The concentration of the nanoparticles was determined by using the data obtained from an axial inductively coupled plasma (ICP) atomic emission spectrometer machine. The cells were then synchronized in the G1 phase by serum starvation.[44] Subsequently, they were released into the complete medium before PERS experiments. The cell viability assay was conducted by using the XTT cell viability assay kit (Biotium, Inc.) by following the manufacturer's protocol. Anti-HO-1 antibody was purchased from abcam and the GAPDH, secondary mouse and rabbit antibodies were from Santa Cruz Biotechnology.

(f) *In vitro* PERS measurements

PERS spectra from the cells, during cisplatin exposure at different concentrations, were collected in a time dependent manner. Here, an auto-injection system was used to administrate the drug through the live cell chamber. The effect of drug treatment was monitored at different times after drug administration by collecting the PERS spectra. The spectra were measured with a 1200 lines/mm grating using a Renishaw inVia Raman spectrometer. The laser beam (785 nm) was directed into a microscope *via* a series of reflecting lenses and apertures, where it was focused onto the sample using a 50*x*/0.75 N. A. objective. The back-scattered signals from the samples were collected using a CCD detector in the range of 450 to 3000 cm^{-1} with an integration time of 10 s. The spectra were processed by the removal of the spectral background. Here, cubic spline interpolation is used for the baseline fit by manually selecting the points representative of the background. Dark-field microscopy images were simultaneously acquired using a Lumenera's infinity2 CCD digital camera.

(g) *In silico* analysis

In silico analysis of HO-1 expression in head and neck cancer and normal head and neck cells was performed using Oncomine (https://www.oncomine.org/resource/login.html) (Fig. S7 in the ESI†). Reporter ID and platform for datasets used were as follows: gene rank 1921 the samples were analyzed on Human Genome U133 Plus 2.0.

Conflicts of interest

There are no conflicts to declare.

Acknowledgements

This work was supported by the National Science Foundation, Division of Chemistry, CHE-1608801 grant.

Notes and references

1 S. R. Panikkanvalappil, M. A. El-Sayed and I. H. El-Sayed, in *Head and Neck Cancer: Multimodality Management*, ed. J. Bernier, Springer International Publishing, Cham, 2016, pp. 827–844, DOI: 10.1007/978-3-319-27601-4_51.
2 H. Kang, A. Kiess and C. H. Chung, *Nat. Rev. Clin. Oncol.*, 2015, **12**, 11–26.
3 R. J. Sanderson and J. A. D. Ironside, *BMJ*, 2002, **325**, 822–827.
4 J. Bernier, S. M. Bentzen and J. B. Vermorken, *Nat. Rev. Clin. Oncol.*, 2009, **6**, 266.
5 S. H. Huang and B. O'Sullivan, *Med. Oral Patol. Oral Cir. Bucal*, 2013, **18**, E233–E240.
6 J. B. Vermorken, R. Mesia, F. Rivera, E. Remenar, A. Kawecki, S. Rottey, J. Erfan, D. Zabolotnyy, H.-R. Kienzer, D. Cupissol, F. Peyrade, M. Benasso, I. Vynnychenko, D. De Raucourt, C. Bokemeyer, A. Schueler, N. Amellal and R. Hitt, *N. Engl. J. Med.*, 2008, **359**, 1116–1127.
7 E. S. Davidi, T. Dreifuss, M. Motiei, E. Shai, D. Bragilovski, L. Lubimov, M. J. J. Kindler, A. Popovtzer, J. Don and R. Popovtzer, *Head Neck*, 2017, **40**, 70–78.
8 P. M. Takahara, A. C. Rosenzweig, C. A. Frederick and S. J. Lippard, *Nature*, 1995, **377**, 649.
9 M. H. Hanigan and P. Devarajan, *Cancer Ther.*, 2003, **1**, 47–61.
10 L. Astolfi, S. Ghiselli, V. Guaran, M. Chicca, E. D. I. Simoni, E. Olivetto, G. Lelli and A. Martini, *Oncol. Rep.*, 2013, **29**, 1285–1292.
11 A. Yakirevitch, Y. P. Talmi, Y. Baram, R. Weitzen and M. R. Pfeffer, *Br. J. Cancer*, 2005, **92**, 1611.
12 Q. X. Tan, H. L. Wang, Y. L. Hu, M. R. Hu, X. G. Li, Aodengqimuge, Y. F. Ma, C. Y. Wei and L. Song, *Cancer Sci.*, 2015, **106**, 1023–1032.
13 T. W. Miller, J. S. Isenberg and D. D. Roberts, *Chem. Rev.*, 2009, **109**, 3099–3124.
14 N. A. Gandini, M. E. Fermento, D. G. Salomón, J. Blasco, V. Patel, J. S. Gutkind, A. A. Molinolo, M. M. Facchinetti and A. C. Curino, *Exp. Mol. Pathol.*, 2012, **93**, 237–245.
15 B. Wegiel, D. Gallo, E. Csizmadia, C. Harris, J. Belcher, G. M. Vercellotti, N. Penacho, P. Seth, V. Sukhatme, A. Ahmed, P. P. Pandolfi, L. Helczynski, A. Bjartell, J. L. Persson and L. E. Otterbein, *Cancer Res.*, 2013, **73**, 7009.
16 M. Kourti, W. G. Jiang and J. Cai, *Oxid. Med. Cell. Longevity*, 2017, **2017**, 9326454.
17 V. Myroshnychenko, J. Rodríguez-Fernández, I. Pastoriza-Santos, A. M. Funston, C. Novo, P. Mulvaney, L. M. Liz-

Marzán and F. J. García de Abajo, *Chem. Soc. Rev.*, 2008, **37**, 1792–1805.
18 P. L. Stiles, J. A. Dieringer, N. C. Shah and R. P. Van Duyne, *Annu. Rev. Anal. Chem.*, 2008, **1**, 601–626.
19 S. R. Panikkanvalappil, S. M. Hira, M. A. Mahmoud and M. A. El-Sayed, *J. Am. Chem. Soc.*, 2014, **136**, 15961–15968.
20 S. R. Panikkanvalappil, M. James, S. M. Hira, J. Mobley, T. Jilling, N. Ambalavanan and M. A. El-Sayed, *J. Am. Chem. Soc.*, 2016, **138**, 3779–3788.
21 G. Bodelón, V. Montes-García, C. Costas, I. Pérez-Juste, J. Pérez-Juste, I. Pastoriza-Santos and L. M. Liz-Marzán, *ACS Nano*, 2017, **11**, 4631–4640.
22 L. A. Lane, X. Qian and S. Nie, *Chem. Rev.*, 2015, **115**, 10489–10529.
23 N. Hooshmand, H. S. Mousavi, S. R. Panikkanvalappil, A. Adibi and M. A. El-Sayed, *Nano Today*, 2017, **17**, 14–22.
24 W. P. Wuelfing, S. M. Gross, D. T. Miles and R. W. Murray, *J. Am. Chem. Soc.*, 1998, **120**, 12696–12697.
25 S. R. Panikkanvalappil, N. Hooshmand and M. A. El-Sayed, *Bioconjugate Chem.*, 2017, **28**, 2452–2460.
26 S. Behzadi, V. Serpooshan, W. Tao, M. A. Hamaly, M. Y. Alkawareek, E. C. Dreaden, D. Brown, A. M. Alkilany, O. C. Farokhzad and M. Mahmoudi, *Chem. Soc. Rev.*, 2017, **46**, 4218–4244.
27 H. Dehari, Y. Ito, T. Nakamura, M. Kobune, K. Sasaki, N. Yonekura, G. Kohama and H. Hamada, *Cancer Gene Ther.*, 2002, **10**, 75.
28 J. Robbins, S. M. Dilwortht, R. A. Laskey and C. Dingwall, *Cell*, 1991, **64**, 615–623.
29 B. Kang, L. A. Austin and M. A. El-Sayed, *ACS Nano*, 2014, **8**, 4883–4892.
30 S. R. Panikkanvalappil, S. M. Hira and M. A. El-Sayed, *Chem. Sci.*, 2016, **7**, 1133–1141.
31 L. A. Austin, B. Kang and M. A. El-Sayed, *J. Am. Chem. Soc.*, 2013, **135**, 4688–4691.
32 L. Wei, Y. Yu, Y. Shen, M. C. Wang and W. Min, *Proc. Natl. Acad. Sci. U. S. A.*, 2013, **110**, 11226.
33 S. Hong, T. Chen, Y. Zhu, A. Li, Y. Huang and X. Chen, *Angew. Chem., Int. Ed.*, 2014, **53**, 5827–5831.
34 H. Zhang, C. Wang, H. L. Sun, G. Fu, S. Chen, Y. J. Zhang, B. H. Chen, J. R. Anema, Z. L. Yang, J. F. Li and Z. Q. Tian, *Nat. Commun.*, 2017, **8**, 15447.
35 S. Park, A. Wieckowski and M. J. Weaver, *J. Am. Chem. Soc.*, 2003, **125**, 2282–2290.
36 M. A. Tadayyoni and M. J. Weaver, *Langmuir*, 1986, **2**, 179–183.
37 H. Yang, Y. Yang and S. Zou, *J. Phys. Chem. C*, 2007, **111**, 19058–19065.
38 S. Park, P. Yang, P. Corredor and M. J. Weaver, *J. Am. Chem. Soc.*, 2002, **124**, 2428–2429.
39 I. Mrozek, C. Pettenkofer and A. Otto, *Surf. Sci.*, 1990, **238**, 192–198.
40 C. d. l. Torre, A. Toscani, C. Marín-Hernández, J. A. Robson, M. C. Terencio, A. J. P. White, M. J. Alcaraz, J. D. E. T. Wilton-Ely, R. Martínez-Máñez and F. Sancenón, *J. Am. Chem. Soc.*, 2017, **139**, 18484–18487.
41 M. Tinajero-Trejo, K. J. Denby, S. E. Sedelnikova, S. A. Hassoubah, B. E. Mann and R. K. Poole, *J. Biol. Chem.*, 2014, **289**, 29471–29482.
42 D. L. Morse, H. Gray, C. M. Payne and R. J. Gillies, *Mol. Cancer Ther.*, 2005, **4**, 1495.
43 P. N. Sisco and C. J. Murphy, *J. Phys. Chem. A*, 2009, **113**, 3973–3978.
44 B. Kang, L. A. Austin and M. A. El-Sayed, *Nano Lett.*, 2012, **12**, 5369–5375.